Hindawi
Wireless Communications and Mobile Computing
Volume 2022, Article ID 7940993, 12 pages
https://doi.org/10.1155/2022/7940993

Research Article

Precoded IM-OFDM-SS for Underwater Acoustic Communication

Zeyad A. H. Qasem[1], **Hussein A. Leftah**[2], **Haixin Sun**[1] and **Hamada Esmaiel**[1,3]

[1]*Department of Information and Communication, School of Informatics, Xiamen University, Xiamen 316005, China*
[2]*Basrah Engineering Technical College, Southern Technical University, Iraq*
[3]*Electrical Engineering Department, Faculty of Engineering, Aswan University, Aswan 81542, Egypt*

Correspondence should be addressed to Hamada Esmaiel; h.esmaiel@aswu.edu.eg

Received 16 December 2021; Revised 30 January 2022; Accepted 18 February 2022; Published 9 March 2022

Academic Editor: Abdul Basit

The nature of the multipath channel and the peak-to-average power ratio (PAPR) are regarded as the main challenges restricting the design of a multicarrier reliable underwater acoustic (UWA) communication. This paper proposes a new scheme, precoded index modulation orthogonal frequency division modulation spread spectrum (IM-OFDM-SS), for UWA communication. The precoded IM-OFDM-SS is proposed to increase the transmission efficiency and exploit the spreading and multipath diversities and, at the same time, reduce the PAPR to achieve a reliable communication system. Two different precoders, discrete Hartley transform (DHT) and discrete cosine transform (DCT), are utilized in the proposed scheme and compared with the conventional IM-OFDM-SS scheme. Simulation and real experimental results demonstrate the outperformance of the proposed precoded IM-OFDM-SS in comparison to the conventional benchmarks in terms of PAPR and bit error rate (BER) performance.

1. Introduction

An underwater acoustic (UWA) channel is regarded as one of the most complicated media in use due to its challenging effects. The main challenges of UWA channels are represented by the long-delay effect and doubly selective channel caused by the oceanic environment [1, 2]. As the receiver, the signal is superimposed due to the substantial multipath effect causing a superposition of the signal at the receiver side rising a severe intersymbol interference (ISI) in the ocean environment. Therefore, exhaustive processing must be employed at the receiving end for equalizing and estimating the channel to ensure the reliability of UWA communication.

As a result, researchers are working hard to establish a reliable UWA communication with an acceptable data rate in that environment using two main modulation techniques, which are single-carrier and multicarrier modulations. On the one hand, single-carrier modulation was proven to be capable of dealing with the ISI since the adaptive equalizer can be employed, e.g., a decision feedback equalizer with a recursive least squares algorithm [3]. Furthermore, the use of correcting coding can also provide communication with better quality [4]. The main drawback of a single-carrier system is the high-complexity process required for recovering the channel's effects at the receiving end. On the other hand, multicarrier modulation is presented to avoid that concern; it can mitigate the delay spread and bandwidth limitation of the UWA channel with less required processing. A multicarrier modulation system is able to recover the channel using a significantly low-complexity equalizer, but unfortunately, the significant Doppler effect leads to severe intercarrier interference (ICI) [5, 6].

Orthogonal frequency division multiplexing (OFDM) can be considered the finest choice which can effectively overcome the UWA channel effects. That is due to its ability to deal with the long multipath spread UWA channel with low-complex frequency-domain equalization; this means that, different from signal carrier systems, OFDM does not require a complicated time-domain equalization [5, 7, 8]. Despite those advantages, OFDM still has a problem with the high peak-to-average power ratio (PAPR) in UWA communication, limited spectral efficiency, and performance deterioration in communication systems with harsh channels [9].

Consequently, to overcome the OFDM PAPR performance and increase its resilience to multipath fading channels, channel-independent unitary precoders were utilized in OFDM systems [10]. Intensive research on using different unitary precoders such as Walsh-Hadamard transforms (WHT), discrete Hartley transform (DHT) [11], and discrete cosine transform (DCT) [12, 13] showed that system complexity and PAPR reduction level are mainly determined by the used unitary precoder.

Recently, the index modulation OFDM (IM-OFDM) was proposed [14–17] to overcome the intercarrier interference (ICI) that existed in the conventional OFDM scheme as well as improve its spectral efficiency. Unlike OFDM, the subcarriers in OFDM-IM are classified to be active or idle, where the data is carried physically by digital modulation via the active subcarriers and, at the same time, the index of the active subcarriers conveys additional information bits. OFDM-IM can provide better BER performance in low-to-medium data rate systems compared to OFDM. The maximum likelihood (ML) detector, regarded as an optimal detector, is employed at the receiver for jointly detecting the index of active subcarriers and modulated data. Apart from the high computational complexity of the ML receiver, the channel estimation error leads to dramatic deterioration of the performance of the ML decoder [18]. That issue becomes exhaustive in such untrusted communication systems like UWA communication. That is because of the dependence between the detection of data symbols and active subcarriers. In other words, the erroneous detection of active subcarriers leads to the incorrect decision of the data symbols [19]. Therefore, detecting the varied index of active subcarriers must be guaranteed at the receiving end by having perfect knowledge on the channel, which is one of the main difficulties in UWA communication.

On the other hand, the index modulation OFDM spread spectrum (IM-OFDM-SS) [18] was presented to improve the diversity gain of OFDM-IM. Unlike OFDM-IM, IM-OFDM-SS activates all subcarriers to transmit the modulated data symbols, but it spreads each data symbol across different subcarriers using a predefined spreading code. Specifically, the information bits are divided into two parts: one part is transmitted via the index of that predefined spreading code and the other part is carried by the spread modulated data symbols. Therefore, additional diversity is gained as the data symbols are spread across different subcarriers. Additionally, the maximal ratio combining (MRC) detector can straightforwardly be employed at the receiving end for performing low-complex detection as well as avoiding the issues of the ML detector related to the channel estimation susceptibility [18]. Despite those advantages, IM-OFDM-SS and OFDM-IM inherit the high PAPR from conventional OFDM systems.

In order to overcome the PAPR issue of OFDM and harvest higher diversity gain, X-transform IM-OFDM-SS has been presented in [20]. The higher performance of PAPR in that scheme is acquired by the low-complex X-transform matrix, composed of the discrete Fourier transform (DFT) matrix and DHT matrix. The channel effects in that scheme are recovered in the time-domain pseudo-noise (PN) packet inserted for estimation tasks as well as guard interval. The enhanced performance provided by X-transform IM-OFDM-SS can only be guaranteed when considering the slow-varied UWA channel as the overhead packets are inserted at the beginning and at the end of each symbol. Moreover, inserting additional overhead packets might lead to deteriorating the structure of the X-transform matrix.

Motivated by those advantages offered by IM-OFDM-SS and X-transform IM-OFDM-SS, the contribution of this paper is to propose a new scheme called precoded IM-OFDM-SS to maximize the efficiency of the limited bandwidth of the UWA channel, decrease the higher PAPR, and suppress the residual ICI. Discrete cosine transform (DCT) type II and Hartley transform (DHT) are used as a spreading matrix for the new precoded IM-OFDM-SS. Unlike X-transform IM-OFDM-SS [20], the proposed schemes insert the overhead packets in the frequency domain to track the fast-varied UWA channel effects. Although the PAPR performance is a little bit deteriorated compared to our proposed scheme in [20], we believe that the proposed schemes are environment dependent making them very attractive for the untrusted UWA communication systems. Thanks to the precoding and spreading techniques of the new schemes, the information symbols are distributed over all new scheme subcarriers; hence, the symbol of a highly attenuated subcarrier can be recovered from the other subcarriers. The new precoded IM-OFDM-SS uses the unequal attenuation effect over the spread subcarrier symbols to avoid the underwater burst error and improve the UWA communication reliability. The rest of this paper is structured as follows: the system model, including the transmitter and the receiver of the proposed schemes, is presented in Section 2. The system performance analysis is studied in Section 3. Simulation and experimental results are shown in Section 4, and the conclusion of this paper is presented in Section 5.

2. System Model

The proposed IM-OFDM-SS structure is shown in Figure 1, letting the input of the bit splitter be B data bits. The B bits are divided into G groups, and each group has m bits, $m = B/G$. Bit splitter divides bits of each group $g \in \{1,\cdots,G\}$ into two subgroups $P_1^{(g)}$ and $P_2^{(g)}$. $P_1^{(g)}$ is transmitted via the index of the selected spreading code $\mathbf{c}_{i^{(g)}}$ out of the preconfigured code set $\mathbb{C} = \{\mathbf{c}_1,\cdots,\mathbf{c}_n\}$, where $i^{(g)} \in \{1,\cdots n\}$ is the index of the g-th group spreading code. The $\mathbf{c}_{i^{(g)}}$ length is n. The other subgroup $P_2^{(g)}$ is mapped into the $s^{(g)} \in \chi$ symbol, χ is any M-ary digital modulation with a unit average power, and $P_2^{(g)} = \log_2(M)$. The modulated constellation symbols $s^{(g)}$ will be spread over the spreading code $\mathbf{c}_{i^{(g)}}$ selected using $P_1^{(g)}$ index bits as follows:

$$\mathbf{x}^g = \left[x_1^{(g)}, \cdots, x_n^{(g)}\right]^T = \left[s^{(g)}c_{i^{(g)},1}, \cdots, s^{(g)}c_{i^{(g)},n}\right]^T. \quad (1)$$

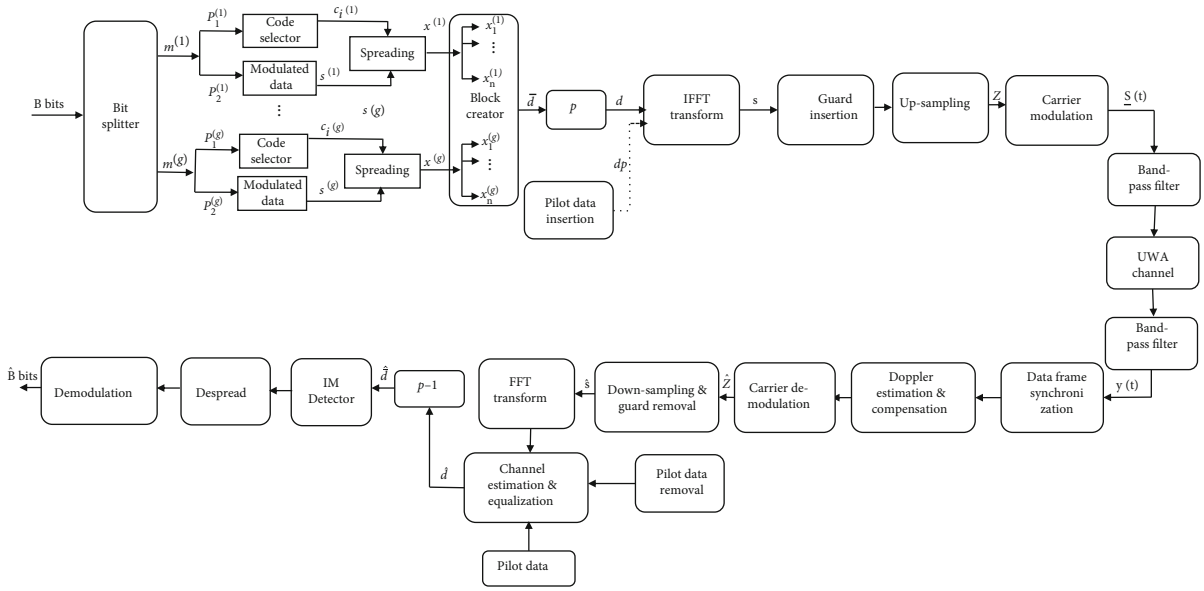

Figure 1: Structure of the UWA precoded IM-OFDM-SS system.

In this paper, to relax the receiver complexity, the maximum size of $\mathbb{C}$ spreading codes is normally restricted to be n since it must be mutually orthogonal, and we can consider 5the orthogonal codes of Walsh or Zadoff-Chu (ZC) [18]. The data symbol vector $[\bar{\mathbf{d}}]_{\mathscr{M}\times 1} = [\mathbf{x}^1, \mathbf{x}^2, \cdots, \mathbf{x}^G]$ is generated by concatenating $\mathbf{x}^g$ of all groups, and the total transmitted bits via the new precoded IM-OFDM-SS can be written as

$$\mathscr{N} = G \times (\log_2(n) + \log_2(M)). \tag{2}$$

Unlike the conventional IM-OFDM-SS, the proposed precoded IM-OFDM-SS multiplies the vector of spread data symbol $\bar{\mathbf{d}}$ by a precoding matrix; $\mathscr{P}$ resulting in the precoded data symbol noted $\mathscr{d}$, noted by $\mathscr{d} = \mathscr{P}\bar{\mathbf{d}}$. In this paper, DCT type II and DHT are considered precoding matrices $\mathscr{P}, \mathscr{P} \in \mathbb{R}^{\mathscr{M}\times\mathscr{M}}$; the (r, l) entries of DCT and DHT are given in (3) and (4), respectively. In both cases, the $\mathscr{P}$ matrix is invertible and has a flexible size which can be any positive integer; its entries have the same magnitude. Consequently, all IM-OFDM-SS data symbols 5are equally spread over $\mathscr{M}$ with significant diversity gain compared to the conventional IM-OFDM-SS.

$$\mathscr{p}_{r,l} = \begin{cases} \sqrt{\dfrac{2}{\mathscr{M}}}\ \cos\left(\dfrac{(l-1)(2l-1)\pi}{2\mathscr{M}}\right), & r > 1, \\ \sqrt{\dfrac{1}{\mathscr{M}}}, & r = 1, \end{cases} \tag{3}$$

$$\rho_{r,l} = \cos\left(\frac{2\pi rl}{\mathscr{M}}\right) + \sin\left(\frac{2\pi rl}{\mathscr{M}}\right). \tag{4}$$

For channel estimation purposes, pilot tones $\mathscr{d}_{\mathbf{P}}$ are multiplexed with the $\mathscr{d}$ to estimate the doubly selective UWA channel. The resulted vector $\mathscr{d}_{\mathbf{T}} \in \mathbb{C}^{N\times 1}$ including data, pilots, and null subcarriers is fed into the OFDM modulator as the inverse fast Fourier transform (IFFT) is used for modulating information symbols. Then, the cyclic prefix (CP) is inserted as a guard interval resulting in the transmitted baseband signal expressed as follows:

$$\mathbf{s}(t) = \sum_{n=-N/2}^{N/2-1} \mathscr{d}_{\mathbf{T}}[n] e^{j2\pi n\Delta \mathrm{ft}}, \tag{5}$$

where Δf is the OFDM subcarrier frequency spacing. Then, the baseband signal transmitted over the UWA channel will be processed by upconversion including upsampling and carrier modulation. The underwater channel can be written as [21]

$$\mathbf{h}(t,\tau) = \sum_{\rho=1}^{\mathrm{L}} \alpha_\rho(\mathrm{t})\delta\Big(\tau - \big(\tau_\rho - \beta_\rho \mathrm{t}\big)\Big), \tag{6}$$

where $\alpha_\rho(t)$, $\tau_\rho(t)$, $\delta(t)$, and β_ρ denote the time-varying amplitudes of the path ρ, delays of L multipath components, Dirac delta function, and Doppler scaling factor (DSF), respectively. The received passband signal is

$$\mathbf{y}(\mathbf{t}) = \mathrm{Re}\left\{\sum_{\rho=1}^{L} \alpha_\rho \left[\sum_{n=-\mathrm{N}/2}^{\mathrm{N}/2-1} \mathscr{d}_T[n] e^{j2\pi n\Delta f\left(t+\beta t-\tau_\rho\right)}.\mathrm{p}\left(\mathrm{t}+\beta-\tau_\rho\right)\right] \times e^{j2\pi f_c\left(t+\beta t-\tau_\rho\right)}\right\} + \mathbf{v}(\mathbf{t}), \tag{7}$$

where $\mathbf{v}(\mathbf{t}) \sim \mathscr{CN}(0, \sigma^2)$ is the passband additive white Gaussian noise (AWGN). f_c and $p(t)$ denote the carrier frequency and pulse shaping filter, respectively. Root-raised cosine-type pulse shaping filters are used in both the transmitter and the receiver. In (7), each path of the received

signal is scaled in $(T \sim T/(1+\beta))$; T is the OFDM symbol duration. Also, a Doppler shift $e^{j2\pi\beta f_n t}$ is affecting every subcarrier. The frequency-dependent Doppler shift causes a critical ICI in the UWAC. To mitigate the ICI effect, the two-step Doppler estimation and compensation in [21] are adopted in this paper where two low-frequency modulation (LFM) segments are used as preamble and postamble to coarsely estimate the DSF at the receiver end. The DSF is estimated by a cross-correlation between $\mathbf{y}(\mathbf{t})$ and those two known segments, preamble and postamble. Cross-correlation operation will give a signal with two peaks; the first one is utilized for synchronization. The difference between first and second cross-correlation peaks is used to find the length of the received signal $\mathscr{B}'$. By comparing $\mathscr{B}'$ with the length of transmitted signal length $\mathscr{B}$ which is supposed to be known, the DSF can be estimated as

$$\beta' = \frac{\mathscr{B}}{\mathscr{B}'} - 1. \tag{8}$$

The received signal is resampled at the receiving end as in (7) at $(1+\beta')f_s$, where f_s is the original sampling frequency used at the transmitter side. The resampled received signal under a resampling factor β' is $\underline{\mathbf{z}}(t) = \mathbf{y}(t/(1+\beta'))$, $\mathbf{z}(\mathbf{t}) = \mathrm{Re}\,(\underline{\mathbf{z}}(\mathbf{t})e^{j2\pi f_c t})$. Considering $(1+\beta)/(1+\beta') = 1$, $\mathbf{z}(\mathbf{t})$ can be expressed as

$$\mathbf{z}(\mathbf{t}) \approx e^{j2\pi\beta - \beta'/1+\beta' f_c t} \times \sum_{n=-N/2}^{N/2-1} \left\{ \boldsymbol{d}_T[n] e^{j2\pi n \Delta \mathrm{ft}} \times \left[\sum_{\rho=1}^{L} \alpha_\rho e^{-j2\pi f_n \tau_\rho} p\left(t - \tau_\rho\right) \right] \right\} + \bar{\mathbf{v}}(\mathbf{t}), \tag{9}$$

where $\bar{\mathbf{v}}(\mathbf{t}) \sim \mathscr{CN}(0, \sigma^2)$ is the AWGN in the baseband. The expression of the frequency-independent Doppler shift is given following (9) by

$$\mathscr{E} = \frac{\beta - \beta'}{1+\beta'} f_c. \tag{10}$$

The ε term in (10) is called carrier frequency offset (CFO) when the narrowband is considered. The CFO is estimated by minimizing the null subcarriers' energy. To explain the CFO estimation in the precoded IM-OFDM-SS, we use the null subcarrier of the received data, after resampling each OFDM data block. Assume a vector $\mathbf{f}_n$ of $(N+L)\times 1$, where $\mathbf{f}_n = [1, e^{j2\pi n/N}, \cdots\cdots, e^{j2\pi n(N+L-1)/N}]^T$ and a $(N+L)\times(N+L)$ diagonal matrix $\boldsymbol{\zeta}(\mathscr{E}) = \mathrm{diag}\,\{[1, e^{j2\pi T_n \mathscr{E}}, \cdots\cdots\cdots, 1, e^{j2\pi T_n (N+L-1)\mathscr{E}}]\}$; $\mathscr{E}$ is the residual CFO, and $T_n = T/N$ is the sample's duration. The energy of the null subcarrier whose locations are well known is used as a cost function, and the CFO can be obtained as

$$\hat{\mathscr{E}} = \arg\min_{\mathscr{E}} \left\{ \sum_{n \in \mathscr{S}_N} \left| \mathbf{f}_n^{\mathscr{H}} \boldsymbol{\zeta}^{\mathscr{H}}(\mathscr{E}) \hat{\mathbf{z}} \right|^2 \right\}. \tag{11}$$

The collected $N+L$ samples after resampling of each block are $\hat{\boldsymbol{z}} = [\hat{z}(0), \cdots\cdots\cdots, \hat{z}(N+L-1)]^T$. After CFO estimation and compensation, the signal of the n-th subcarrier is given by

$$\hat{\mathbf{s}}[n] = \mathbf{f}_n^{\mathscr{H}} \boldsymbol{\zeta}^{\mathscr{H}}\left(\hat{\mathscr{E}}\right) \hat{\mathbf{z}} = H(n) \hat{\boldsymbol{d}}_{\mathbf{T}}[n] + \bar{\mathbf{v}}_{\mathbf{n}}, \tag{12}$$

where $H = \sum_{\rho=1}^{L} \alpha_\rho e^{-j2\pi f_n \tau_\rho}$ is the channel frequency response, $\bar{\mathbf{v}}_{\mathbf{n}}$ is the resulting noise of the n-th subcarrier, and $\mathscr{H}(.)$ is the Hermitian transpose. Using $\hat{\mathbf{s}}[n]$, channel estimation is performed based on pilot symbols located as predefined. Without loss of generality, orthogonal matching pursuit (OMP) [22] is adopted in this paper for underwater channel estimation, and the minimum means square error (MMSE) is used for equalization. After removing the overhead packets from the MMSE equalizer output, the resultant signal $\hat{\boldsymbol{d}} \in \mathbb{C}^{\mathscr{M}\times 1}$ is the received precoded estimated data. The IM-OFDM-SS demapping extracts the physically transmitted data encapsulated in the index of the spreading code. First, the dispreading matrix $\boldsymbol{\mathscr{P}}^{\mathscr{H}}$ is used to extract the transmitted data symbols $\hat{\hat{\boldsymbol{d}}}$ (noted by $\hat{\hat{\mathbf{d}}} = \boldsymbol{\mathscr{P}}^{\mathscr{H}} \hat{\boldsymbol{d}}$).

The maximum ratio combining (MRC) detector is employed, as shown in Figure 2, for detecting the received information bits. Each vector $\hat{\mathbf{x}}^{(g)} \in \mathbb{C}^{n\times 1}$, picked from $\hat{\hat{\boldsymbol{d}}}$, which is corresponding to the subgroup g, is dispread by all predefined spreading codes used at the transmitting end. Thus, the output of the l-th code, $l \in \{1, \cdots n\}$, can be expressed as follows:

$$\Delta_l = \sum_{k=1}^{n} \hat{x}^{(g)} c_{l^{(g)},k}. \tag{13}$$

Therefore, $P_1^{(g)}$ can be found using (13) as follows:

$$\hat{i}^{(g)} = \arg \max_l |\Delta_l|^2. \tag{14}$$

Finally, the output of dispreading $\hat{\mathbf{x}}^{(g)}$ using $\hat{i}^{(g)}$ is corresponding to $P_2^{(g)}$.

3. Performance Analysis

This section evaluates the proposed precoded IM-OFDM-SS scheme in terms of pairwise error probability (PEP) and coding and diversity gains. The conditional PEP of the estimated $\hat{\boldsymbol{d}}$ data to the transmitted data $\boldsymbol{d}$ is given by

$$P\left(\mathbf{d} \longrightarrow \frac{\hat{\mathbf{d}}}{\mathbf{H}}\right) = Q\left(\sqrt{\frac{\left\| \mathbf{H}\boldsymbol{\mathscr{P}}\left(\mathbf{d} - \hat{\mathbf{d}}\right) \right\|^2}{2N_0}}\right), \tag{15}$$

where $Q(.)$ is the Gaussian tail probability [23]. Using the Q-function, an alternative form of (15) can be expressed as

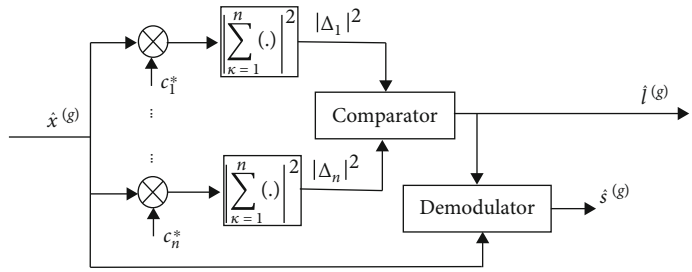

Figure 2: MRC detector of the precoded IM-OFDM-SS.

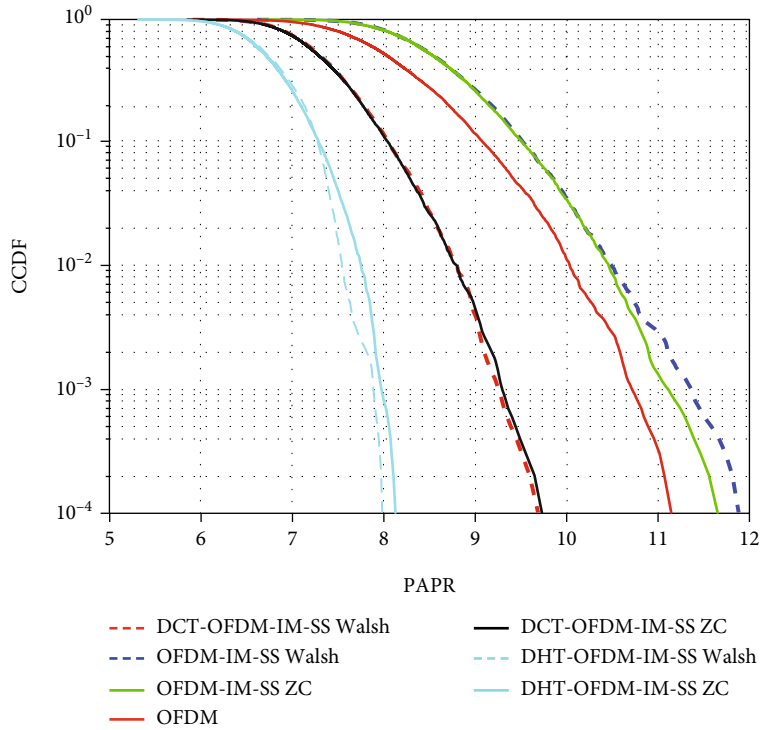

Figure 3: PAPR performance comparison.

follows [23]:

$$P\left(\mathbf{d} \longrightarrow \frac{\widehat{\mathbf{d}}}{\mathbf{H}}\right) = \frac{1}{\pi}\int_0^{\pi/2} e^{\left(-\frac{\mu}{4N_0\ \sin^2\varnothing}\right)} d\varnothing, \tag{16}$$

where $\mu = \|\mathbf{H}\mathscr{P}(\mathbf{d}-\widehat{\mathbf{d}})\|^2$ which can be rewritten as $\mu = \sum_{i=1}^{\mathscr{M}}\sigma_i|h_i|^2$, $\sigma_i = |\boldsymbol{\varphi}_i(\mathbf{d}-\widehat{\mathbf{d}})|^2$, and $\boldsymbol{\varphi}_i$ is the i-th row of $\mathscr{P}$. The unconditional PEP is given by averaging (16) with respect to μ as follows:

$$P\left(\mathbf{d} \longrightarrow \widehat{\mathbf{d}}\right) = \frac{1}{\pi}\int_0^{\pi/2} \aleph_\mu\left(-\frac{1}{4N_0\ \sin^2\varnothing}\right) d\varnothing, \tag{17}$$

where $\aleph_\mu$ is the moment generating function (MGF) of μ. Due to the channel model, the MGF of $\Lambda_i = \sigma_i|h_i|^2$ of μ is $\aleph_{\Lambda_i}(t) = (1-\sigma_i\varphi^2 t)^{-1}$ which gives $\aleph_\mu(t) = \prod_{i=1}^{\mathscr{M}}(1-\sigma_i\varphi^2 t)^{-1}$. Therefore, (17) can be expressed as

$$P\left(\mathbf{d} \longrightarrow \widehat{\mathbf{d}}\right) = \frac{1}{\pi}\int_0^{\pi/2} \prod_{i=1}^{\mathscr{M}} \frac{\sin^2\varnothing}{\sin^2\varnothing + (\sigma_i\varphi^2/4N_0)} d\varnothing. \tag{18}$$

For any precoding matrix $\mathscr{P}$, let us define $\Gamma_{\mathbf{d},\widehat{\mathbf{d}}}$ as the cardinality of a defined set $\mathscr{Q}_{\mathbf{d},\widehat{\mathbf{d}}} = \{i \mid \sigma_i \neq 0\}$, $\Gamma_{\mathbf{d},\widehat{\mathbf{d}}} = |\mathscr{Q}_{\mathbf{d},\widehat{\mathbf{d}}}|$, we can approximate $\sin^2\varnothing(\sin^2\varnothing + (\sigma_i\varphi^2/4N_0))^{-1} \leq (1+(\sigma_i\varphi^2/4N_0))^{-1} \approx 4/\sigma_i\bar{\gamma}$ at high signal-to-noise ratios (SNRs) because $0 \leq \sin^2\varnothing \leq 1$. The integrant of (18) can be approximated as

$$P\left(\mathbf{d} \longrightarrow \widehat{\mathbf{d}}\right) \approx \frac{(\bar{\gamma}/4)^{-\Gamma_{\mathbf{d},\widehat{\mathbf{d}}}}}{2\prod_{i\in\mathscr{Q}_{\mathbf{d},\widehat{\mathbf{d}}}}\sigma_i}. \tag{19}$$

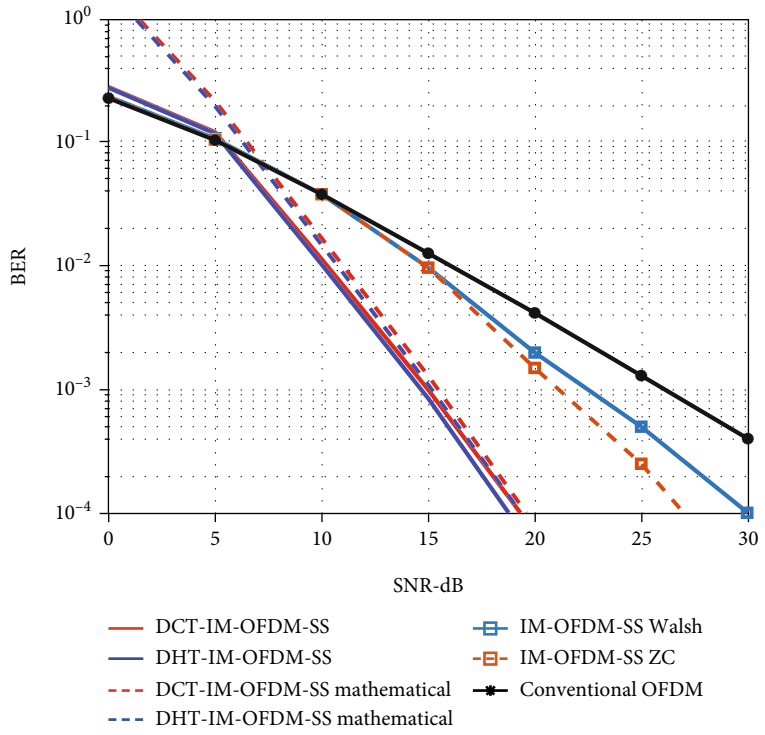

Figure 4: BER performance of the precoded IM-OFDM-SS with the Walsh code as $\mathbf{c}_{i(g)}$.

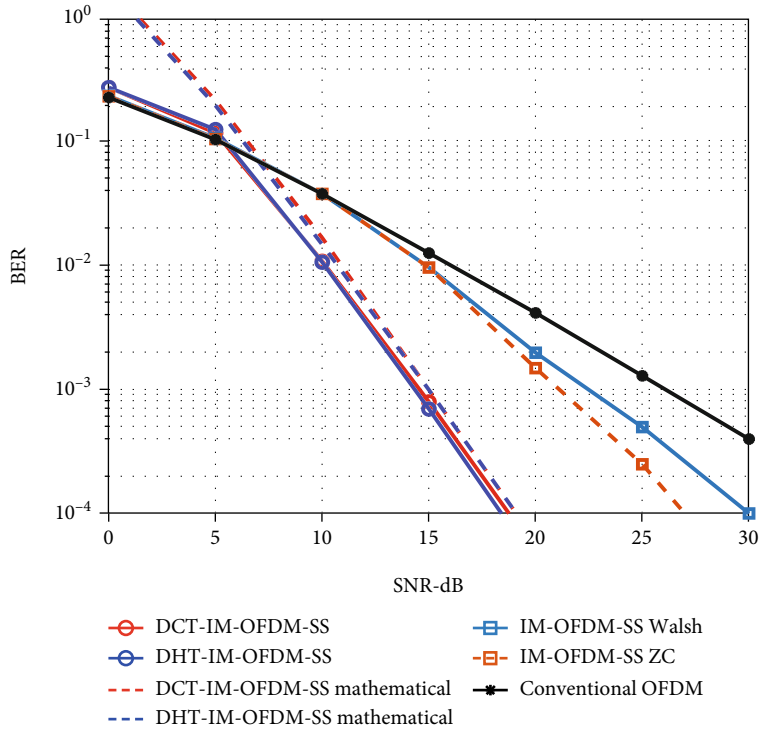

Figure 5: BER performance of the precoded IM-OFDM-SS with the ZC code as $\mathbf{c}_{i(g)}$.

Figure 6: Packet structure.

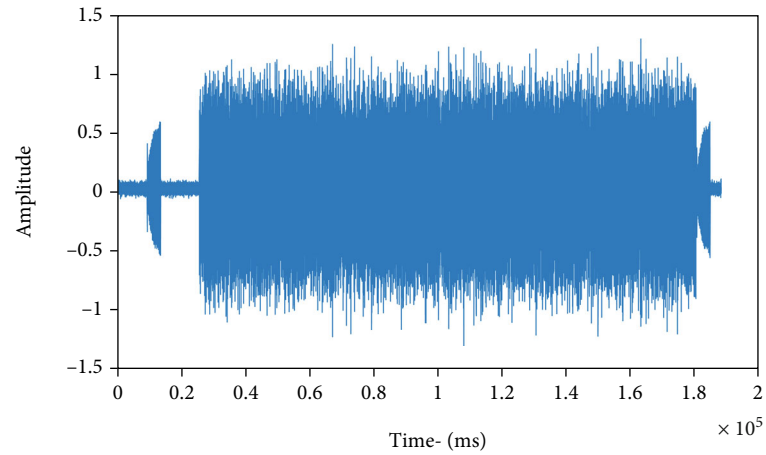

(a)

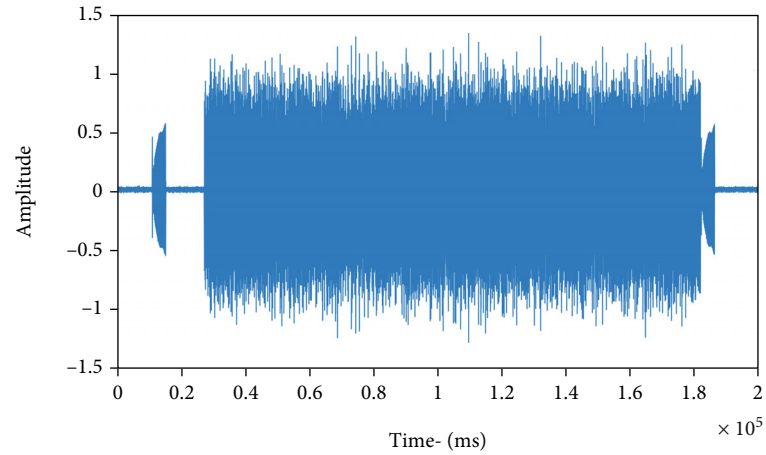

(b)

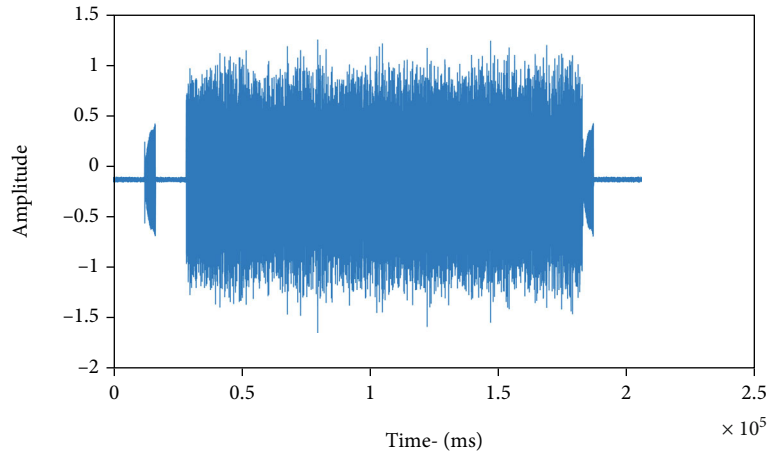

(c)

Figure 7: Continued.

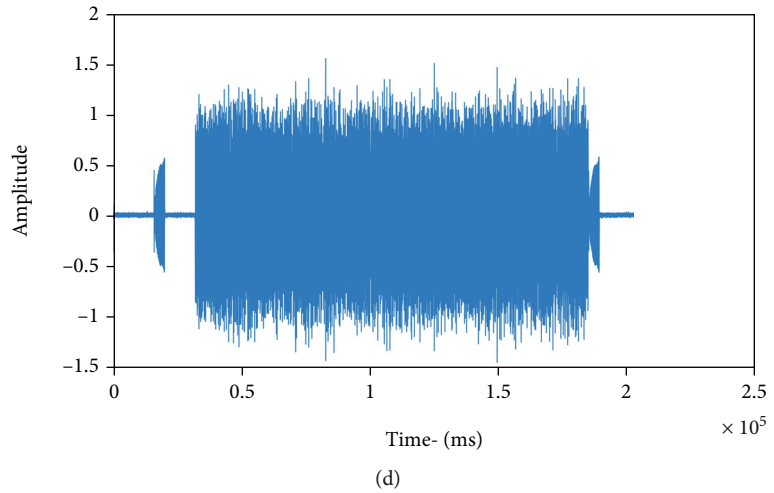

Figure 7: Received signal: (a) DCT-IM-OFDM-SS Walsh; (b) DCT-IM-OFDM-SS ZC; (c) DHT-IM-OFDM-SS Walsh; (d) DHT-IM-OFDM-SS ZC.

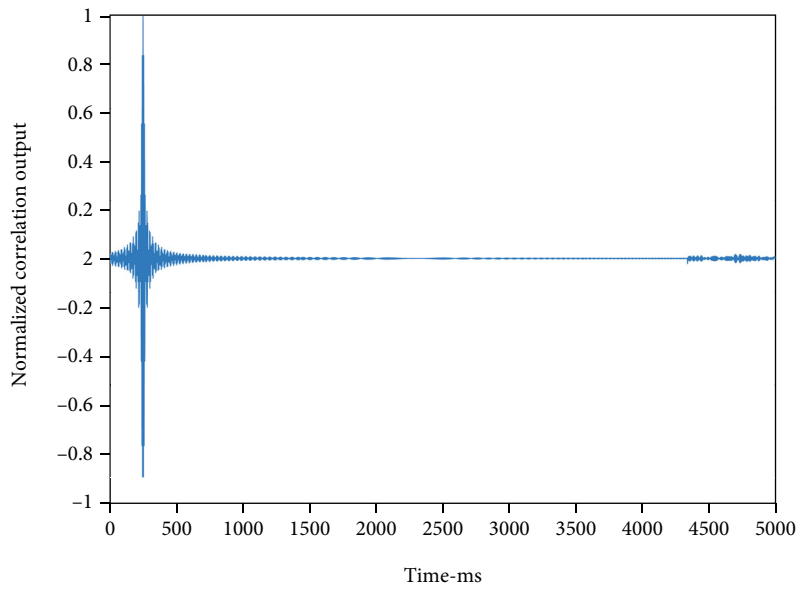

Figure 8: Estimated channel using the preamble correlation—pool experiments.

Therefore, the diversity and coding gains of the precoded IM-OFDM-SS are, respectively, given by

$$\mathcal{G}_e = \min_{\mathbf{d}\neq\hat{\mathbf{d}}} \Gamma_{\mathbf{d},\hat{\mathbf{d}}}, \mathcal{G}_c = \min_{\mathbf{d}\neq\hat{\mathbf{d}},\ \Gamma_{\mathbf{d},\hat{\mathbf{d}}}=\mathcal{G}_e} \left(\prod_{i\in\mathcal{Q}_{\mathbf{d},\hat{\mathbf{d}}}} \sigma_i \right)^{.1/\mathcal{G}_e} \tag{20}$$

Finally, the upper bound BEP can be written based on $P(\mathbf{d} \longrightarrow \tilde{\mathbf{d}})$ evaluation using the union bound theory as follows:

$$P_b \leq \frac{1}{m^{nMG}} \sum_{\mathbf{d}} \sum_{\tilde{\mathbf{d}}} \frac{\mho\left(\mathbf{d}, \hat{\mathbf{d}}\right) (\bar{\gamma}/4)^{-\Gamma_{\mathbf{d},\hat{\mathbf{d}}}}}{2\prod_{i\in\mathcal{Q}_{\mathbf{d},\hat{\mathbf{d}}}} \sigma_i}. \tag{21}$$

Moreover, the use of IM-OFDM-SS instead of IM-OFDM offers additional diversity order since the data of each subcarrier is spread over many subcarriers. The formula of BER given by IM-OFDM-SS is calculated in [18].

4. Simulation and Experimental Results

The proposed precoded IM-OFDM-SS performance is evaluated in terms of BER and PAPR based on simulation and real experimental underwater channels.

4.1. Simulation Evaluation. For the simulation channel, the results are obtained over the 10^5-symbol transmitter over a statistical underwater channel presented in [24]. The proposed precoded IM-OFDM-SS performances are compared with those of the conventional UWA-OFDM [21] and IM-

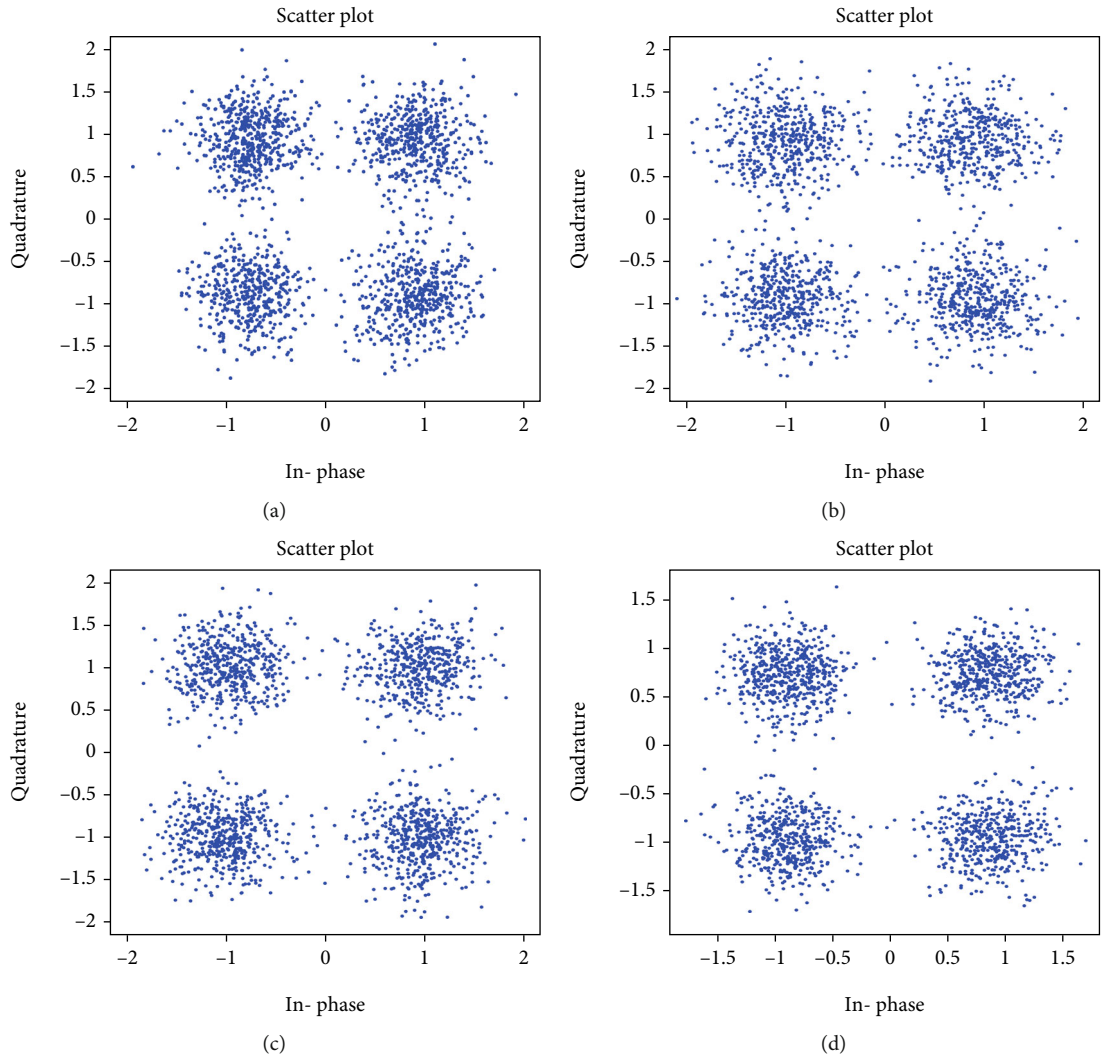

Figure 9: Constellation plot: (a) DCT-IM-OFDM-SS Walsh; (b) DCT-IM-OFDM-SS ZC; (c) DHT-IM-OFDM-SS Walsh; (d) DHT-IM-OFDM-SS ZC—pool experiments.

Table 1: Experimental pool results.

No.	OFDM	IM-OFDM-SS Walsh	IM-OFDM-SS ZC	Proposed DCT Walsh	Proposed DCT ZC	Proposed DHT Walsh	Proposed DHT ZC
1	0.018	0.020	0.020	0.0038	0.0031	0.0035	0.0031
2	0.0096	0.0072	0.0061	0.0021	0.0022	0.0021	0.0021
3	0.027	0.0041	0.0035	0.0035	0.0035	0.0030	0.0033
4	0.026	0.023	0.022	0.0091	0.009	0.0093	0.0088
5	0.0072	0.0061	0.0065	0.00054	0.00052	0.00053	0.00054
Average	0.0176	0.0121	0.0116	0.0038	0.0037	0.0037	0.0036

OFDM-SS [18]. In this simulation and without loss of generality, Walsh and ZC codes are used as spreading codes $\boldsymbol{c}_{i^{(g)}}$.

In simulation demonstration, each block contains $N = 1024$ with a guard interval of 256. For a fair comparison, all communication schemes have the same system data rate, $T = 0.25$ ms, and the bandwidth of 5 kHz; f_c and f_s are set to be 23 kHz and 122.8 kHz, respectively. To guarantee a similar transmitted rate for all communication schemes, the binary phase-shift keying (BPSK) is used with the conventional OFDM and the quadrature amplitude modulation (QAM) is employed for the IM-OFDM-SS and precoded IM-OFDM-SS at $n = 4$. Both the transmitter and receiver are 10 m below the surface with a 0.2 km distance between them. The CFO = 0.02 and $\beta = 3e - 4$ are used. The RRC filter has been used at the transmitter and receiver with a roll-off of 0.55. Figure 3 shows the PAPR complementary cumulative

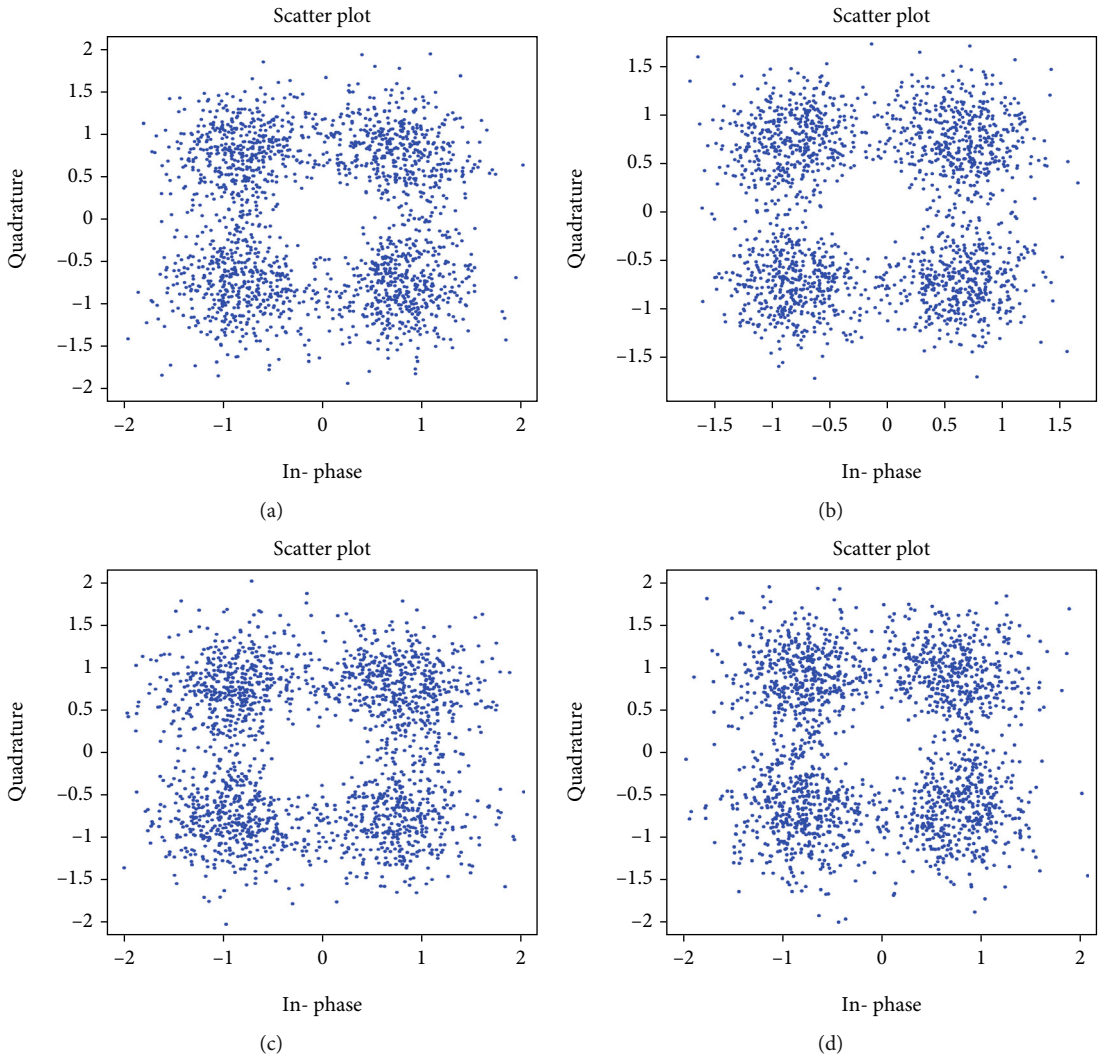

Figure 10: Constellation plot: (a) DCT-IM-OFDM-SS Walsh; (b) DCT-IM-OFDM-SS ZC; (c) DHT-IM-OFDM-SS Walsh; (d) DHT-IM-OFDM-SS ZC—shallow-water experiments.

Table 2: Experimental shallow water results.

No.	OFDM	IM-OFDM-SS Walsh	IM-OFDM-SS ZC	Proposed DCT Walsh	Proposed DCT ZC	Proposed DHT Walsh	Proposed DHT ZC
1	0.042	0.043	0.042	0.015	0.014	0.021	0.009
2	0.031	0.022	0.026	0.0083	0.0072	0.007	0.008
3	0.061	0.046	0.040	0.0091	0.0098	0.0084	0.0072
4	0.008	0.006	0.01	0.002	0.003	0.001	0.001
5	0.0096	0.0090	0.006	0.0079	0.0068	0.008	0.0085
Average	0.0303	0.0252	0.0248	0.0085	0.0082	0.0076	0.0067

distribution function (CCDF) performance. As shown, the IM-OFDM-SS when using $\mathbf{c}_{i^{(g)}}$ Walsh or ZC is suffering from higher PAPR compared with the conventional OFDM, while the proposed schemes including both DCT-based precoding and DHT-based precoding offer about 1.5 dB and 3 dB superiority compared with the conventional schemes, respectively. The low PAPR of the precoded IM-OFDM-SS schemes is because the precoded schemes overcome the input information symbol superposition which forms each OFDM sample. DHT-based precoding offers better PAPR than DCT-based precoding. This is because of the similarity of the IFFT and the DHT where some matrix kernels are canceling each one another leading to avoiding the superposition of the input data symbols due to the combined DHT-IFFT [11, 12, 20, 25]. Figures 4 and 5 show the BER performance of precoded schemes when using $\mathbf{c}_{i^{(g)}}$ Walsh and ZC, respectively. The

proposed precoded IM-OFDM-SS in both cases offers more than 5~10 dB compared with IM-OFDM-SS and traditional UWA-OFDM. The BER improvement in the precoded IM-OFDM-SS is because of spreading symbol data vectors over all subcarriers enabling the recovery of highly attenuated symbols from the others which are well received. Both precoded IM-OFDM-SS using the Walsh code and ZC code achieve maximum diversity with slight superiority when using the ZC code due to the large Euclidean distance in ZC code vectors. Moreover, it is worth mentioning here that in low SNR, below 5 dB, there is a slightly small BER gain in the conventional scheme in comparison to the proposed scheme. This is because the power in the case of the proposed precoded system is spread over two transforms instead of a single transform in the case of a conventional scheme, making the system more susceptible to error in the case of extremely low SNR. However, this has no impact on the superiority of our proposed scheme in the practical scenarios as it achieves about 9 dB SNR gain at 10^{-4} BER in comparison to the conventional IM-OFDM-SS.

4.2. Pool Experimental Results. The proposed scheme's effectiveness is also evaluated over a UWA real channel. This experiment was carried out at Xiamen University, where a pool of size 18 m × 5 m is used for transmitting a signal between one transmitting and one receiving hydrophone. The depth of the transmitter and the receiver is 1.2 m beneath the water's surface, and 7 m distance is separating them. The transmitted packet is shown in Figure 6, five packets with ten symbols in each frame have been transmitted with FFT size, guard interval, f_c, f_s, effective bandwidth, symbol duration, and data rate being set similar to parameters mentioned above in the case of the simulated channel Section 4.1. The used structure of the packet to be practically transmitted is shown in Figure 6 where two LFM segments are transmitted before and after the packet. Those two segments are used for synchronization and DSF estimation as explained in Section 2. A vector of zeros is inserted between the preamble and data vectors to prevent the inference while an optional zero vector can be inserted between the data vector and postamble too. The received data corresponding to $\mathbf{y}(\mathbf{t})$ in (6) is shown in Figure 7 including the DHT-based and DCT-based precoded IM-OFDM-SS for one frame based on $\mathbf{c}_{i(g)}$ of Walsh and ZC codes.

In practical real experiments, a cross-correlation between the received signal and the well-known preamble and postamble segments is first performed; the first resulted peak was used for synchronization while the difference between the first and the second peaks is utilized to evaluate the DSF as in (8). The output of cross-correlation is shown in Figure 8. After estimating and compensating the DSF, the signal shows the output of the correlator between the preamble and the received signal processed as explained in Section 2. Figure 9 shows the constellation of the received signal of the proposed precoded schemes after despreading the signal following (14). It is worth mentioning that IM-OFDM-SS is practically evaluated in this paper for underwater communication for the first time. Precoded IM-OFDM-SS offers better performance than conventional OFDM and IM-OFDM-SS schemes in both cases of using the Walsh and ZC codes. The DHT-based precoded IM-OFDM-SS scheme slightly outperforms the DCT-based precoded IM-OFDM-SS scheme. In fact, under a perfect linear communication system that is completely free of nonlinear devices, all the aforementioned precoded systems should have the same diversity degree and ultimately the same BER performance. However, as the system is not perfectly linear, the DHT precoded IM-OFDM-SS has better BER performance than the other precoders as it has less PAPR as mentioned above, and consequently, the interference due to the performance of the nonlinear device is reduced. The proposed scheme is compared to the traditional UWA-OFDM in Table 1.

4.3. Shallow Water Experimental Results. The experiment took place in Xiamen, China, at the port of Xiamen. Five frames with ten symbols in each frame have been transmitted; the transmitter and receiver are separated by 106 meters, with depth of 5 meters beneath the sea surface. FFT size, guard interval, f_c, f_s, effective bandwidth, symbol duration, and data rate were set similar to the parameters mentioned above in Sections 4.1 and 4.2. The sea's channel is considered to be a harsh channel, so to guarantee communication reliability, conventional coding with the rate of 2/3 and interleaving are adopted. The received signal is processed similar to Section 4.2 where the constellation of the received signal after (14) is shown in Figure 10, and the experimental results are shown in Table 2. The performance of the proposed schemes confirms the effectiveness of the proposed schemes over the practical UWA channel.

5. Conclusion

This paper proposed a new scheme called precoded IM-OFDM-SS for UWA communication. The IM-OFDM-SS data symbols are spread over all other subcarriers; hence, the reliability of the UWA communication system can be improved. Thanks to the precoding and spreading scheme, the proposed IM-OFDM-SS increases the transmit diversity, domesticates the spreading and multipath diversities of the UWA channel, and reduces the PAPR. The performance of the proposed schemes has been evaluated over simulation and experimental results. The new scheme outperformed the conventional OFDM multicarrier modulation scheme currently used in the UWAC and the new conventional IM-OFDM-SS proposed for the next 5G mobile networks which are not previously practically evaluated over the UWA channel. Field measurements and simulation results clearly show how the proposed precoded IM-OFDM-SS is suitable for the UWAC.

Data Availability

The authors declare that the data used to support the findings of this study will be available from the corresponding author upon request.

Conflicts of Interest

The authors declare that they have no conflicts of interest.

Acknowledgments

This work is supported by the National Natural Science Foundation of China (61671394), the Fundamental Research Funds for the Central Universities (20720170044), and the Science and Technology Program of Shenzhen, China (JSGG20170414090428464).

References

[1] M. E. Bayrakdar, "Cooperative communication based access technique for sensor networks," *International Journal of Electronics*, vol. 107, no. 2, pp. 212–225, 2020.

[2] M. E. Bayrakdar, "A smart insect pest detection technique with qualified underground wireless sensor nodes for precision agriculture," *IEEE Sensors Journal*, vol. 19, no. 22, pp. 10892–10897, 2019.

[3] M. Stojanovic, J. A. Catipovic, and J. G. Proakis, "Phase-coherent digital communications for underwater acoustic channels," *IEEE Journal of Oceanic Engineering*, vol. 19, no. 1, pp. 100–111, 1994.

[4] E. Sozer, J. G. Proakis, and F. Blackmon, "Iterative equalization and decoding techniques for shallow water acoustic channels," in *MTS/IEEE Oceans 2001. An Ocean Odyssey. Conference Proceedings (IEEE Cat. No.01CH37295)*, vol. 4, pp. 2201–2208, Honolulu, HI, USA, December 2001.

[5] Y. V. Zakharov and A. K. Morozov, "OFDM transmission without guard interval in fast-varying underwater acoustic channels," *IEEE Journal of Oceanic Engineering*, vol. 40, no. 1, pp. 144–158, 2015.

[6] J. Li and Y. V. Zakharov, "Efficient use of space-time clustering for underwater acoustic communications," *IEEE Journal of Oceanic Engineering*, vol. 43, no. 1, pp. 173–183, 2017.

[7] M. Stojanovic, "OFDM for underwater acoustic communications: adaptive synchronization and sparse channel estimation," in *2008 IEEE International Conference on Acoustics, Speech and Signal Processing*, vol. 1no. 6, pp. 5288–5291, Las Vegas, NV, USA, 2008.

[8] B. Li, J. Huang, S. Zhou et al., "MIMO-OFDM for high-rate underwater acoustic communications," *IEEE Journal of Oceanic Engineering*, vol. 34, no. 4, pp. 634–644, 2009.

[9] G. Rojo and M. Stojanovic, "Peak-to-average power ratio (PAR) reduction for acoustic OFDM systems," in *OCEANS 2009*, pp. 1–7, Biloxi, MS, USA, October 2009.

[10] J. Tao, "DFT-precoded MIMO OFDM underwater acoustic communications," *IEEE Journal of Oceanic Engineering*, vol. 43, no. 3, pp. 805–819, 2017.

[11] H. A. Leftah and S. Boussakta, "Efficient modulation scheme for OFDM system with ZP and MMSE equalizer," in *2013 IEEE International Conference on Communications (ICC)*, pp. 4703–4707, Budapest, Hungary, June 2013.

[12] H. A. L. Al-Sodani, *New OFDM schemes based on orthogonal transforms for mobile communications systems*, Doctoral dissertation, Newcastle University, 2013.

[13] H. A. Leftah and S. Boussakta, "Novel OFDM based on C-transform for improving multipath transmission," *IEEE Transactions on Signal Processing*, vol. 62, no. 23, pp. 6158–6170, 2014.

[14] H. V. Poor, "Orthogonal frequency division multiplexing with index modulation," in *2012 IEEE Global Communications Conference (GLOBECOM)*, pp. 4741–4746, Anaheim, CA, USA, 2012.

[15] E. Basar, "Index modulation techniques for 5G wireless networks," *IEEE Communications Magazine*, vol. 54, no. 7, pp. 168–175, 2016.

[16] E. Basar, M. Wen, R. Mesleh, M. Di Renzo, Y. Xiao, and H. Haas, "Index modulation techniques for next-generation wireless networks," *IEEE Access*, vol. 5, pp. 16693–16746, 2017.

[17] M. Wen, B. Zheng, K. J. Kim et al., "A survey on spatial modulation in emerging wireless systems: research progresses and applications," *IEEE Journal on Selected Areas in Communications*, vol. 37, no. 9, pp. 1949–1972, 2019.

[18] Q. Li, M. Wen, E. Basar, and F. Chen, "Index modulated OFDM spread spectrum," *IEEE Transactions on Wireless Communications*, vol. 17, no. 4, pp. 2360–2374, 2018.

[19] J. Choi, "Coded OFDM-IM with transmit diversity," *IEEE Transactions on Communications*, vol. 65, no. 7, pp. 3164–3171, 2017.

[20] Z. A. Qasem, H. A. Leftah, H. Sun, J. Qi, and H. Esmaiel, "X-transform time-domain synchronous IM-OFDM-SS for underwater acoustic communication," *IEEE Systems Journal*, pp. 1–12, 2021.

[21] B. Li, S. Zhou, M. Stojanovic, L. Freitag, and P. Willett, "Multicarrier communication over underwater acoustic channels with nonuniform Doppler shifts," *IEEE Journal of Oceanic Engineering*, vol. 33, no. 2, pp. 198–209, 2008.

[22] N. Lin, H. Sun, E. Cheng, J. Qi, X. Kuai, and J. Yan, "Prediction based sparse channel estimation for underwater acoustic OFDM," *Applied Acoustics*, vol. 96, pp. 94–100, 2015.

[23] M. K. Simon and M.-S. Alouini, *Digital Communication over Fading Channels*, John Wiley & Sons, 2005.

[24] P. Qarabaqi and M. Stojanovic, "Statistical characterization and computationally efficient modeling of a class of underwater acoustic communication channels," *IEEE Journal of Oceanic Engineering*, vol. 38, no. 4, pp. 701–717, 2013.

[25] Z. A. Qasem, J. Wang, X. Kuai, H. Sun, and H. Esmaiel, "Enabling unique word OFDM for underwater acoustic communication," *IEEE Wireless Communications Letters*, vol. 10, no. 9, pp. 1886–1889, 2021.